Eur. Phys. J. D (2016) 70: 39
DOI: 10.1140/epjd/e2016-60419-0

THE EUROPEAN PHYSICAL JOURNAL D

Regular Article

Tunable modulation instability in metamaterials with pseudo-quintic nonlinearity, self-steepening effect and delayed Raman response

Rongcao Yang[a], Xuemin Min, Jinping Tian, and Wenmei Zhang

College of physics & Electronics Engineering, Shanxi University, Taiyuan 030006, P.R. China

Received 18 July 2015 / Received in final form 23 November 2015
Published online 18 February 2016 – © EDP Sciences, Società Italiana di Fisica, Springer-Verlag 2016

Abstract. Modulation instability (MI) in metamaterials induced by pseudo-quintic nonlinearity, self-steepening effect along with delayed Raman response (DRR) is investigated and expression for MI gain is presented by linear stability method. Compared to the previous results with saturable nonlinearity, it is found that the MI without DRR may occur in four primary cases with different threshold behaviors depending on the combination of dispersion and nonlinearity and the competition of pseudo-quintic nonlinearity and self-steepening effect. This implies that we may manipulate or tune the MI by adjusting the power and frequency of incident waves at will. In addition, we consider the influence of DRR on MI and find that the DRR leads to additional regions where it entirely governs the MI gain, besides the primary ones where the self-steepening and the pseudo-quintic nonlinearity dominate the MI gain. Moreover, the DRR makes MI happen in three new cases exhibiting monotonous growth with perturbation frequency, which means that it is possible to observe MI at arbitrary high frequency. Finally, we confirm the analytical results by numerical simulations. The obtained results may be useful for manipulating or tuning the MI in metamaterials and provide more ways to generate ultrashort pulses with ultrahigh repetition rate.

1 Introduction

Modulation instability (MI) is a remarkable nonlinear phenomenon that has been extensively studied in various nonlinear dispersive systems especially in nonlinear optics [1–8]. It is well-known that MI arises from the interaction between dispersion and nonlinearity and results in a continuous wave evolving into a train of ultrashort pulses [1–3]. MI is usually considered to be a source of soliton trains and related to supercontinuum generation. In optical fibers, it has been demonstrated that MI usually occurs in the anomalous group velocity dispersion (GVD) regime [1–3] except for some special cases in the presence of the four-order dispersion, relaxing self-focusing nonlinearity or cooperation propagation of two optical beams, where MI may occur in normal- or zero-GVD regimes [4–9].

Over the past decade, considerable attention has been paid to the MI in nonlinear metamaterials after some dynamical models for ultrashort pulse propagation in metamaterials were established, which demonstrated that the dispersive magnetic permeability leads to some significant differences between metamaterials and conventional materials [10–14]. For example, the self-steepening effect in metamaterials may be positive or negative, which can cause the pulse to steepen along its leading or trailing edge and the spectrum to split asymmetrically with blueshifted or redshifted peaks, different from that in optical fiber where the self-steepening effect only steepens the trailing edge of the pulses and causes the spectrum redshift. Such differences result in new properties in the formation of solitons and the generation of MI. Some bright, dark and combined solitary waves in metamaterials have been investigated [15–18]. The previous study shows that the anomalous self-steepening effect can be used to manipulate the MI [19], the second-order nonlinear dispersion induced by the dispersive magnetic permeability makes MI possible in the normal-GVD regime, or in the case of no GVD in metamaterials [20], the saturable nonlinearity suppresses the MI gain in abnormal dispersion regime and the fourth-order dispersion induces the additional sideband of MI [21–24], and the combination of cubic-quintic nonlinearities increases the MI gain in metamaterials [23]. It has been demonstrated that in metamaterials, the third-order nonlinear polarization $\chi^{(3)}$ can cause pseudo-$\chi^{(5)}$ nonlinear effect, which enhances cubic nonlinear effect in negative index region, while quenches the cubic nonlinearity in positive index region [11–13]. This means that the pseudo-quintic nonlinearity may play a different role in the occurrence of MI. On the other hand, DRR in metamaterials has seldom been studied except that Boardman et al. [25] investigated the propagation of temporal soliton with Raman scattering and magnetooptic control, and

[a] e-mail: sxdxyrc@sxu.edu.cn

Xiang et al. [14] discussed the controllable Raman soliton self-frequency shift in nonlinear metamaterials. In fibers, it has been identified that DRR significantly alters the properties of MI, which makes MI occur in all dispersion regimes and exerts different influences on the Stokes and anti-Stokes components [26–28]. To the best of our knowledge, MI induced by the combination of the pseudo-quintic nonlinearity and the self-steepening effect along with the DRR in metamaterials remains unexplored.

The aim of this paper is to present the new features of MI induced by the combination of the pseudo-quintic nonlinearity, the self-steepening effect and the DRR in self-focusing and self-defocusing nonlinear metamaterials. Compared to the previous ones that the saturable or quintic nonlinearities are considered [21,22], it is found that there exist a rich variety of MI in metamaterials with different threshold behaviors depending on the combinations of dispersion and nonlinearity and the competition of the pseudo-quintic nonlinearity and the self-steepening, which means that one can make the MI happen in different regions with different gains and spectral widths by tuning the power and frequency of the incident waves. In addition, we discuss the additional features of MI induced by the DRR, showing that the DRR dominates MI gain in the additional regions and additional cases, and the self-steepening and the pseudo-quintic nonlinearity effects entirely govern the MI gain in primary ones. The obtained results in this paper may provide new ways to manipulate or tune the MI gain in metamaterials.

2 Theoretical model and linear stability analysis

2.1 Theoretical model

The propagation of ultrashort pulses in uniform nonlinear metamaterials is described by an extended nonlinear Schrödinger equation [14,25]

$$\frac{\partial A}{\partial Z} = -\frac{i\beta_2}{2}\frac{\partial^2 A}{\partial T^2} + \frac{\beta_3}{6}\frac{\partial^3 A}{\partial T^3} + i\,\gamma_0 \times \left[|A|^2 A - \sigma|A|^4 A + iS_1\frac{\partial}{\partial T}(|A|^2 A) - T_R A\frac{\partial |A|^2}{\partial T}\right], \tag{1}$$

where $A(Z,T)$ is the complex envelope of electric field in the moving reference frame $Z = z$ and $T = t - z/v_g$.

$$\beta_2 = [\alpha\gamma + \omega(\varepsilon\gamma' + \mu\alpha')/2 - 1/v_g^2]/k_0$$

and

$$\beta_3 = 3[\omega(\varepsilon\gamma'' + \mu\alpha'')/6 + (\alpha\gamma' + \alpha'\gamma)/2 - \beta_2/v_g]/k_0$$

are the respective coefficients of the GVD and the third-order dispersion. $\gamma_0 = \omega_0\mu_r\chi^{(3)}/2cn$ and $S_1 = (1+\gamma/\mu)/\omega_0 - 1/k_0 v_g$ stand for the Kerr nonlinearity and the self-steepening effect, and $\sigma = \gamma_0/2k_0$ denotes the pseudo-quintic nonlinearity that arises from $\chi^{(3)}$ nonlinear polarization, respectively. T_R is the DRR parameter independent of frequency for a given pulse length [14,25]. Here $v_g = 2k_0/\omega(\varepsilon\gamma + \mu\alpha)$ is the group velocity, k_0 is the wave number at the carrier frequency ω_0, ε and μ are the dispersive dielectric permittivity and magnetic permeability, respectively.

$$\alpha = \partial\,[\omega\varepsilon(\omega)]/\partial\omega|_{\omega=\omega_0}, \quad \alpha' = \partial^2\,[\omega\varepsilon(\omega)]/\partial\omega^2\big|_{\omega=\omega_0},$$
$$\gamma = \partial\,[\omega\mu(\omega)]/\partial\omega|_{\omega=\omega_0}, \quad \gamma' = \partial^2\,[\omega\mu(\omega)]/\partial\omega^2\big|_{\omega=\omega_0},$$

and

$$n = \pm\sqrt{\varepsilon(\omega)\mu(\omega)}.$$

The mentioned-above linear and nonlinear coefficients in equation (1) are directly related to the dispersive magnetic permeability, which is different from those in conventional materials [10–13].

For convenience, we take the transforms $U = A/A_0$, $\tau = T/T_0$ and $\xi = Z/L_D$with $L_D = T_0^2/|\beta_2|$ to rewrite equation (1) in normalized form as below

$$\frac{\partial U}{\partial \xi} = -i\frac{\delta}{2}\frac{\partial^2 U}{\partial \tau^2} + \frac{b_3}{6}\frac{\partial^3 U}{\partial \tau^3} + i\,\vartheta N^2 \times \left[|U|^2 U - p_5|U|^4 U + is_1\frac{\partial}{\partial\tau}(|U|^2 U) - \tau_R U\frac{\partial |U|^2}{\partial\tau}\right], \tag{2}$$

where $b_3 = \mathrm{sgn}[\beta_3]L_D/L_D'$, $p_5 = \sigma A_0^2$, $s_1 = S_1/T_0$ and $\tau_R = T_R/T_0$ are the normalized parameters of the third-order dispersion, the pseudo-quintic nonlinearity, the self-steepening and the DRR, respectively. Here T_0 and A_0 are the respective duration and amplitude of input pulse, $\delta = \mathrm{sgn}[\beta_2] = \pm 1$ denotes normal or abnormal dispersion, and $\vartheta = \mathrm{sgn}[\gamma_0] = \pm 1$ denotes focusing or defocusing nonlinearity, $N^2 = L_D/L_{NL}$ is the soliton order, $L_D = T_0^2/|\beta_2|$, $L_D' = T_0^3/|\beta_3|$ and $L_{NL} = 1/|\gamma_0|A_0^2$ are the lengths of the GVD dispersion, the third-order dispersion and the nonlinearity, respectively.

2.2 Linear stability analysis

Starting from the normalized equation (2), we adopt standard linear stability analysis to investigate the MI in metamaterials with the pseudo-quintic nonlinearity, the self-steepening effect and the DRR. It is easy to find that equation (2) admits the steady-state solution $U(\xi,\tau) = \sqrt{P_0}\exp[i\,\vartheta(P_0 - p_5P_0^2)\xi]$, where P_0 is the initial power. Introducing a perturbation $a(\xi,\tau)$ ($|a| \ll \sqrt{P_0}$) into the steady-state solution and inserting the perturbed solution into equation (2), one can obtain a linearized equation for $a(\xi,\tau)$

$$\frac{\partial a}{\partial \xi} = -i\frac{\delta}{2}\frac{\partial^2 a}{\partial \tau^2} + \frac{b_3}{6}\frac{\partial^3 a}{\partial \tau^3} + i\,\vartheta P_0 \times \left[(a+a^*) - 2P_0p_5\,(a+a^*) + is_1\left(2\frac{\partial a}{\partial\tau} + \frac{\partial a^*}{\partial\tau}\right) - \tau_R\left(\frac{\partial a}{\partial\tau} + \frac{\partial a^*}{\partial\tau}\right)\right], \tag{3}$$

where a^* is the complex conjugate of a. Separating $a(\xi,\tau) = u(\xi,\tau) + iv(\xi,\tau)$, we can get

$$\frac{\partial u}{\partial \xi} - \frac{\delta}{2}\frac{\partial^2 v}{\partial \tau^2} - \frac{b_3}{6}\frac{\partial^3 u}{\partial \tau^3} + 3\vartheta P_0 s_1 \frac{\partial u}{\partial \tau} = 0, \quad (4)$$

$$\frac{\partial v}{\partial \xi} + \frac{\delta}{2}\frac{\partial^2 u}{\partial \tau^2} - \frac{b_3}{6}\frac{\partial^3 v}{\partial \tau^3} - \vartheta P_0 \left(2u - 4P_0 p_5 u - s_1 \frac{\partial v}{\partial \tau} + 2\tau_R \frac{\partial u}{\partial \tau}\right) = 0. \quad (5)$$

Considering the solutions of equations (4) and (5) in the form [26]

$$\begin{pmatrix} u \\ v \end{pmatrix} = \begin{pmatrix} u_0 \\ v_0 \end{pmatrix} \exp[i(K\xi - \Omega\tau)], \quad (6)$$

where K and Ω represent the wave number and the frequency of the perturbation, respectively. Substituting equation (6) into equations (4) and (5), we can obtain the dispersion relation

$$K = \frac{\Omega^3 b_3}{6} + 2\vartheta P_0 \Omega s_1 - \frac{1}{2} i |\Omega| \times \left[4\delta\vartheta P_0(2P_0 p_5 - 1) - \Omega^2 - 4P_0^2 s_1^2 - i\, 4\delta\vartheta P_0 \Omega \tau_R\right]^{1/2}. \quad (7)$$

It is well-known that the steady-state solution will become unstable when K has a nonzero imaginary part. The expression for the MI gain can be obtained from equation (7)

$$g(\Omega) = 2\mathrm{Im}(K) = \frac{1}{\sqrt{2}}|\Omega| \times \left\{\left[(\Omega^2 - \Omega_c^2)^2 + (4P_0\tau_R\Omega)^2\right]^{1/2} - \Omega^2 + \Omega_c^2\right\}^{1/2}, \quad (8)$$

where $\Omega_c^2 = 4\delta\vartheta P_0(2P_0 p_5 - 1) - 4P_0^2 s_1^2$, and the occurrence condition of MI is given by:

$$\left[(\Omega^2 - \Omega_c^2)^2 + (4P_0\tau_R\Omega)^2\right]^{1/2} - \Omega^2 + \Omega_c^2 > 0. \quad (9)$$

It is straightforward from equations (8) and (9) that the MI gain is a function of Ω, β_2, γ_0, p_5, s_1,τ_R and P_0. In general, τ_R is a constant independent of operational frequency [25], while the parameters β_2, p_5 and s_1 are directly related to $\varepsilon(\omega)$ and $\mu(\omega)$ which are described by the Drude model [29]

$$\varepsilon(\omega) = \varepsilon_0\left[1 - \omega_{pe}^2/\omega(\omega + i\gamma_e)\right]$$

and

$$\mu(\omega) = \mu_0\left[1 - \omega_{pm}^2/\omega(\omega + i\gamma_m)\right],$$

where ε_0 and μ_0 are the respective vacuum permittivity and permeability, ω_{pe} and ω_{pm} are the respective electric and magnetic plasma frequencies, and γ_e and γ_m are the respective electric and magnetic losses. Generally, these losses originate from the intrinsic absorption and resonant nature of the magnetic response, which are inevitable in metamaterials [29,30]. However, several measures have been adopted to reduce or compensate the losses such as optical gain [31,32] and novel fabrication methods [33]. Here we neglect the losses for simplicity. Thus the parameters that contribute to the MI gain can be written as:

$$\beta_2 = \left[\left(1 + 3\tilde{\omega}_p^2/\tilde{\omega}^4\right) - \left(1 - \tilde{\omega}_p^2/\tilde{\omega}^4\right)^2/n^2\right]/cn\omega_{pe}\tilde{\omega},$$
$$p_5 = \chi^{(3)} A_0^2\left(1 - \tilde{\omega}_p^2/\tilde{\omega}^2\right)/4n^2,$$
$$s_1 = \left[1 - \left(\tilde{\omega}_p^2 + \tilde{\omega}^2\right)/\left(\tilde{\omega}_p^2 - \tilde{\omega}^2\right) + \left(\tilde{\omega}_p^2 - \tilde{\omega}^4\right)/n^2\tilde{\omega}^4\right]/T_0\omega_{pe}\tilde{\omega},$$

where $\tilde{\omega} = \omega/\omega_{pe}$, $\tilde{\omega}_p = \omega_{pm}/\omega_{pe}$ and the refractive index $n = \pm(1 - 1/\tilde{\omega}^2)^{1/2}(1 - \tilde{\omega}_p^2/\tilde{\omega}^2)^{1/2}$, respectively. Obviously, these parameters are strongly dependent on the normalized frequency $\tilde{\omega}$. Here we take the typical parameter values $\omega_{pe} = 1.3672 \times 10^{16}$ Hz, $\chi^{(3)} = 10^{-10}$ esu, $T_0 = 50$ fs [34] and present the variations of the parameters n, β_2, p_5 and s_1 with $\tilde{\omega}$ at $\tilde{\omega}_p = 0.8$ for self-focusing and self-defocusing nonlinear metamaterials in Figure 1. It should be noted that β_2, which is independent of nonlinearity, may be either negative or positive in negative index region ($\tilde{\omega} < 0.8$) and always be negative in positive index region ($\tilde{\omega} > 1$). However, p_5 has opposite signs in negative and positive index regions whether for self-focusing or self-defocusing nonlinearity, as shown in Figure 1. This characteristics of the model parameters will directly influence the MI gain and the existence ranges (see Eqs. (8) and (9)). Moreover, the DRR not only contributes to the MI gain, but also is related to the occurrence condition. In the subsequent section, we will focus our attention on the novel features of MI induced by the different combinations of dispersion and nonlinearity in self-focusing ($\vartheta = 1$) and self-defocusing ($\vartheta = -1$) metamaterials with the pseudo-quintic nonlinearity, the self-steepening effect and the DRR.

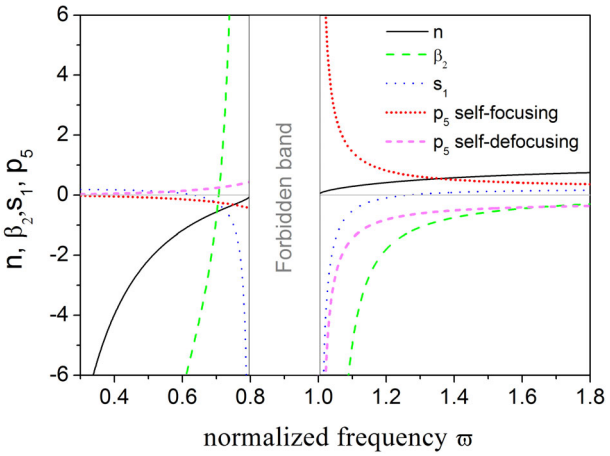

Fig. 1. Variations of n, β_2 and p_5 with the normalized frequency $\tilde{\omega}$ at $\tilde{\omega}_p = 0.8$ in self-focusing and self-defocusing nonlinear metamaterials. Here β_2 is plotted in units of $1/c\omega_{pe}$.

Table 1. The existence regions and occurrence conditions of MI without the DRR.

	MI existence regions $\delta = \mathrm{sgn}[\beta_2], \vartheta = \mathrm{sgn}[\gamma_0]$	MI occurrence conditions
Case A	$\vartheta = 1$ $\delta = -1$ $n < 0$	without constraints
Case B	$\vartheta = 1$ $\delta = -1$ $n > 0$	$P_0 < 1/(2p_5 + s_1^2)$
Case C	$\vartheta = -1$ $\delta = -1$ $n < 0$	$P_0 > 1/(2p_5 - s_1^2)$
Case D	$\vartheta = -1$ $\delta = 1$ $n < 0$	$P_0 < 1/(2p_5 + s_1^2)$

3 Results and discussion

It is easy to see from equation (9) that in the presence of the DRR, the occurrence condition of MI can be satisfied in both negative and positive index regions whether for self-focusing or self-defocusing nonlinear metamaterials, however, in the absence of the DRR, MI can only exist in four different cases for the different combinations of dispersion and nonlinearity in negative and positive index, as will be demonstrated below. The features of MI will be firstly investigated in these four cases without the DRR and then the significance of the DRR in MI gain will be discussed.

3.1 In the absence of the DRR

In the absence of the DRR, i.e. $\tau_R = 0$, the MI gain equation (8) is reduced to

$$g(\Omega) = |\Omega| \sqrt{\Omega_c^2 - \Omega^2} \tag{10}$$

with the requirement

$$\Omega_c^2 = 4\delta\vartheta P_0(2P_0p_5 - 1) - 4P_0^2 s_1^2 > 0, \tag{11}$$

and a peak gain

$$g_{\max} = 2P_0\{\delta\vartheta(2P_0p_5 - 1) - P_0 s_1^2\}, \tag{12}$$

at the maximum growth-rate frequency

$$\Omega_{\max} = \sqrt{2}\left[P_0\delta\vartheta(2P_0p_5 - 1) - P_0^2 s_1^2\right]^{1/2}. \tag{13}$$

It is clear to see that the self-steepening s_1 always suppresses the MI gain regardless of its sign, which is agreement with the previous results [19–24]. Compared to the MI gain spectrum obtained for saturable nonlinearity [21–24], the MI gain (10) shows more interesting dependence on the sign of $\delta\vartheta$ and the sign of p_5. For the case $\delta\vartheta < 0$, negative p_5 promotes the MI gain, while positive p_5 suppresses the MI gain. But it is opposite for the case $\delta\vartheta > 0$. This suggests that the MI features are quite different for different combinations of dispersion and nonlinearity. By analyzing the occurrence requirement (11), we find that the MI in the absence of the DRR can appear in four cases with different constraints depending on the competition of the pseudo-quintic nonlinearity and the self-steepening, as shown in Table 1.

It can be seen from Table 1 that for the self-focusing nonlinearity ($\vartheta = 1$), MI may occur in abnormal GVD ($\delta = -1$) regime of negative index region without any constraints and positive index region with $P_0 < 1/(2p_5 + s_1^2)$; for self-defocusing nonlinearity ($\vartheta = -1$), MI may occur in abnormal ($\delta = -1$) and normal ($\delta = 1$) GVD regimes of negative index region with the occurrence conditions $P_0 > 1/(2p_5 - s_1^2)$ and $P_0 < 1/(2p_5 + s_1^2)$, respectively. In comparison with those in fibers where the MI gain occurs only in the abnormal dispersion regime for self-focusing nonlinearity and in the normal dispersion regime for self-defocusing nonlinearity [3], there exists rich and unusual MI in metamaterials. The physical origin of the unusualness is due to the unique parameter characteristics of metamaterials. From the sign and magnitude of p_5 and s_1 in different index regions shown in Figure 1, it can be seen that pseudo-quintic nonlinearity enhances cubic nonlinearity in negative index region and weakens it in positive index region for both focusing and defocusing nonlinearities, while the magnitude of the self-steepening parameter may be a positive value or a very large negative value, which means these nonlinear effects interact each other to different extent in different regions. Hence the different combinations of p_5 and s_1 in different refraction regions with different nonlinearities can result in rich MI characteristics with different constraints reflecting different competitive relationship, as shown in Table 1. Note that Case A, C and D happen in negative regions of metamterials, which is obviously impossible in fibers. Case B is very similar to the traditional MI in fiber, where the peak value and the band of MI gain increase with the increase of incident power without constraint conditions [3], however, the occurrence of MI in Case B must satisfy the constraint $P_0 > 1/(2p_5 - s_1^2)$ in metamaterials. Physically, these constraints for each case are a competition among P_0, p_5 and s_1. This means there exist the maximum or minimum initial powers for the occurrence of MI in four cases, which is different from that in fibers. In fact, the constraint conditions represent the relationship between the initial power P_0 and the normalized threshold frequency $\tilde{\omega}$ because both p_5 and s_1 are a function of $\tilde{\omega}$ in metamaterials. Therefore we plot the constraints of the initial power P_0 on the normalized frequency $\tilde{\omega}$ for each case in Figure 2, where the curves correspond to the threshold values (P_{th}, $\tilde{\omega}_{\mathrm{th}}$) and the gray areas correspond to all (P_0,$\tilde{\omega}$) which satisfy the occurrence conditions of MI in each case. Obviously, in Figure 2a for Case A, the threshold power $P_{\mathrm{th}} < 0$ which suggests that no power constraint is required for all $\tilde{\omega}$; for the other three cases, MI exhibits threshold requirements. Concretely, for Case B in Figure 2b. MI can occur for $P_0 < P_{\mathrm{th}}$ at a given $\tilde{\omega}$ or $\tilde{\omega} > \tilde{\omega}_{\mathrm{th}}$ at a given P_0, and the threshold power P_{th} increases monotonously with the threshold frequency $\tilde{\omega}_{\mathrm{th}}$; for Case C in Figure 2c, MI can occur for $P_0 > P_{\mathrm{th}}$ at a given $\tilde{\omega}$ or $\tilde{\omega} > \tilde{\omega}_{\mathrm{th}}$ at a given P_0, and the P_{th} decreases monotonously with the increasing $\tilde{\omega}_{\mathrm{th}}$; for Case D in Figure 2d, MI can occur for $P_0 < P_{\mathrm{th}}$ at a given $\tilde{\omega}$ or $\tilde{\omega} < \tilde{\omega}_{\mathrm{th}}$ at a given P_0, and the threshold power P_{th} decreases monotonously with the increasing $\tilde{\omega}_{\mathrm{th}}$.

Naturally, the cutoff frequency $\Omega_c = 2\{\delta\vartheta P_0(2P_0p_5 - 1) - P_0^2 s_1^2\}^{1/2}$ is also the function of P_0 and $\tilde{\omega}$ in each case. Figure 3 illustrates the variations of Ω_c with P_0

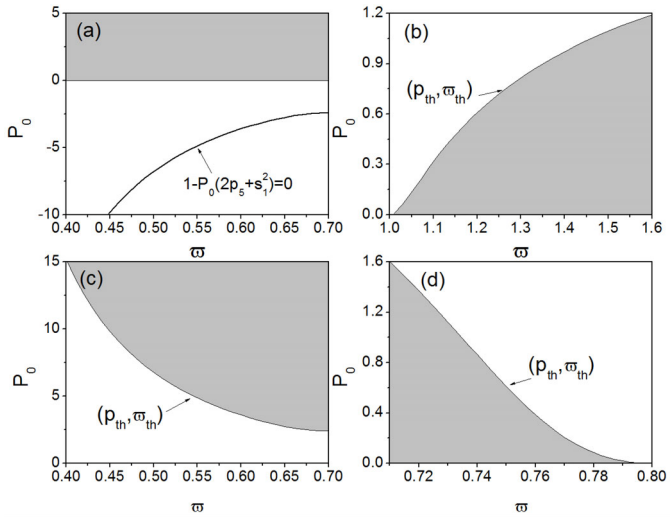

Fig. 2. The constraint conditions of the initial power P_0 and the normalized frequency $\tilde{\omega}$ for each case, respectively.

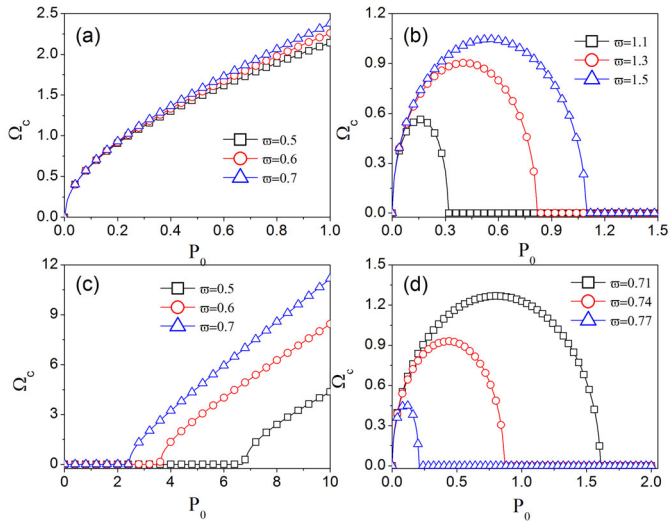

Fig. 3. Variations of the cutoff frequency Ω_c with P_0 and $\tilde{\omega}$ for each case, respectively.

and $\tilde{\omega}$ for each case, respectively. As shown in Figure 3a, due to no threshold requirements in Case A, Ω_c increases monotonously with P_0 and $\tilde{\omega}$ from very low power. For Case B, it is easy to see from Figure 3b that Ω_c increases as $\tilde{\omega}$ increases for a given P_0, and Ω_c increases first and then decreases and cuts off finally as P_0 increases to the threshold power $P_{\rm th}$ for a certain frequency $\tilde{\omega}$. This means the spectrum width experiences a process of first increasing and then decreasing with P_0, which is totally different from that in conventional fibers where the spectrum width increases monotonously with P_0 [3]. Also, unlike Case B, Ω_c increases monotonously with P_0 above the threshold value $P_{\rm th}$ at a certain frequency $\tilde{\omega}$ in Case C, and Ω_c also increases monotonously with $\tilde{\omega}$ at a certain P_0, as shown in Figure 3c. By comparing Case D with Case B, it is found that the variation of Ω_c with P_0 in Case D is similar to

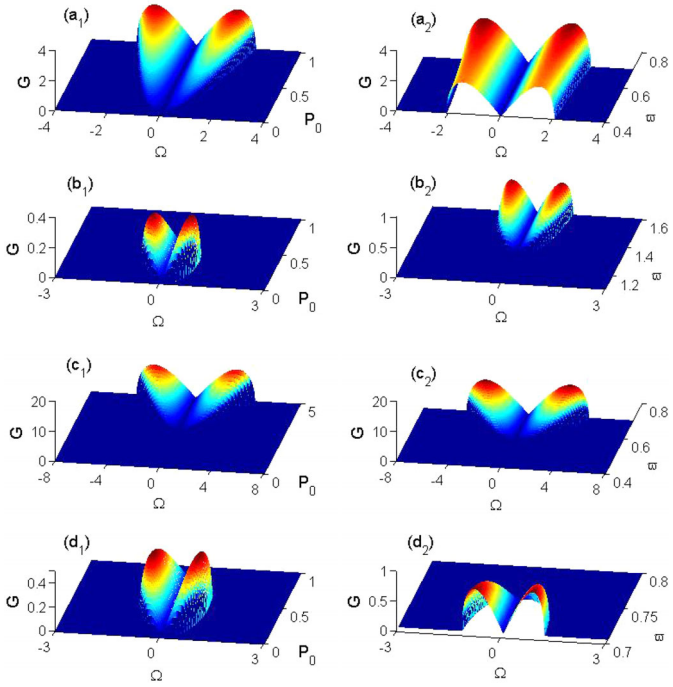

Fig. 4. Variations of the MI gain spectra with the initial power P_0 and the normalized frequency $\tilde{\omega}$ in each case. Here (a_1) $\tilde{\omega} = 0.6$ and (a_2) $P_0 = 1$ are for Case A, (b_1) $\tilde{\omega} = 1.2$ and (b_2) $P_0 = 0.8$ are for Case B, (c_1) $\tilde{\omega} = 0.7$ and (c_2) $P_0 = 5$ are for Case C, (d_1) $\tilde{\omega} = 0.74$ and (d_2) $P_0 = 0.5$ are for Case D, respectively.

that in Case B, namely, as P_0 increases, Ω_c increases first and decreases then and cuts off finally for a certain $\tilde{\omega}$, but the variation of Ω_c with $\tilde{\omega}$ for a given P_0 is opposite to that in Case B.

The differences of the threshold requirements and the cutoff frequencies in each case lead to the difference of the gain spectra. Figure 4 shows the variations of the MI gain spectra with the initial power P_0 and the normalized frequency $\tilde{\omega}$ in each case, respectively. It is clearly seen from Figures 4a_1 and 4a_2 that the peaks and spectral widths increase monotonously with P_0 and $\tilde{\omega}$ without threshold behaviors in spite of different growth rates. As discussed above, there exist different threshold requirements in Case B, C and D. In Case B shown respectively in Figures 4b_1 and 4b_2, MI can occur below the threshold power $P_{\rm th}$ and above the threshold frequency $\tilde{\omega}_{\rm th}$; in Case C shown respectively in Figures 4c_1 and 4c_2, MI can occur above the threshold power $P_{\rm th}$ and above the threshold frequency $\tilde{\omega}_{\rm th}$; in Case D shown respectively in Figures 4d_1 and 4d_2, MI can occur below the threshold power $P_{\rm th}$ and below the threshold frequency $\tilde{\omega}_{\rm th}$. The corresponding threshold power $P_{\rm th}$ at a given $\tilde{\omega}$ and the threshold frequency $\tilde{\omega}_{\rm th}$ at a given P_0 are in full accord with the curves for each case in Figure 2, respectively. Moreover, for each case, the cutoff frequency Ω_c and the gain peak given in equation (12) follow the similar change laws as shown in Figure 3, respectively. It should be pointed out that the spectral features will not change for each case, even though the peak gain and the spectrum width will

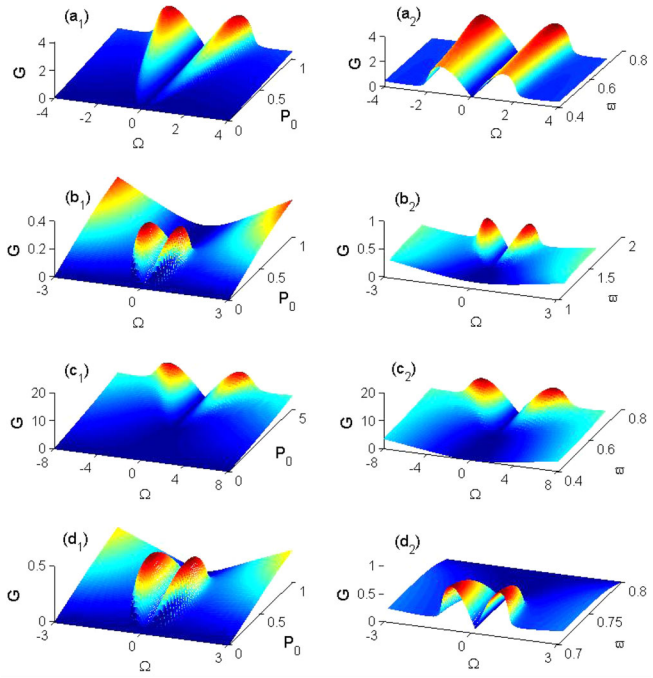

Fig. 5. Gain spectral profiles with $\tau_R = 0.05$ for the corresponding cases in the absence of τ_R. (a_1) and (a_2) for Case A; (b_1) and (b_2) for Case B; (c_1) and (c_2) for Case C; and (d_1) and (d_2) for Case D, respectively. The adopted parameters are the same as in the corresponding subplots of Figure 4 for each case, respectively.

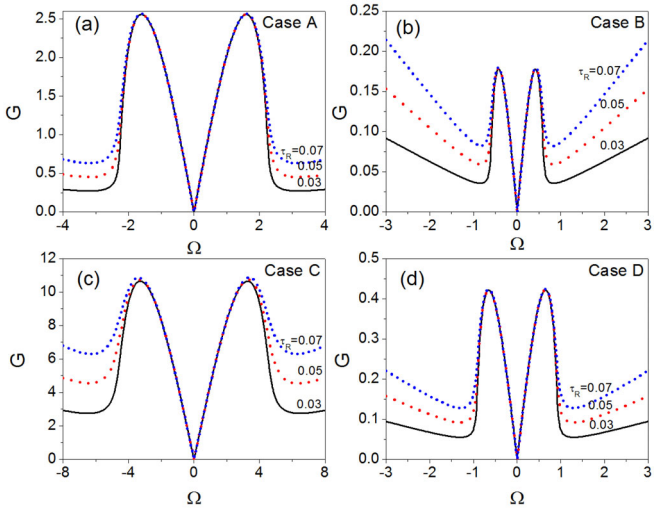

Fig. 6. Gain spectral profiles with different τ_R for (a) Case A $P_0 = 1$, $\tilde{\omega} = 0.6$; (b) Case B $P_0 = 0.5$,$\tilde{\omega} = 1.2$; (c) Case C $P_0 = 5$, $\tilde{\omega} = 0.7$; (d) Case D $P_0 = 0.5$, $\tilde{\omega} = 0.74$, respectively.

change when we change P_0 and $\tilde{\omega}$ of the incident wave. This suggests that we can manipulate or tune the gain and the spectral width by adjusting the initial power and the frequency of the incident waves in each case at will. It is very useful for generating solitary waves in different regions of dispersion and nonlinearity.

3.2 In the presence of the DRR

Let us discuss the features of MI in metamaterials when DRR is taken into account. From equations (8) and (9), it is clear to see that the DRR parameter τ_R affects not only the gain but also the occurrence condition of MI. Owing to the presence of τ_R, equation (9) is always satisfied in all GVD dispersion regimes for self-focusing or self-defocusing nonlinearity, which implies that no threshold requirements are needed. The influences of the DRR on MI gain spectral profiles for the four cases with the DRR are shown in Figure 5. For comparison, here we take the same parameters as in the corresponding subplots of Figure 4 for each case except for $\tau_R = 0.05$. By comparing Figure 5 with Figure 4 correspondingly, it is found that the DRR gives rise to an additional instability region expanding to unlimited high frequency for each case in addition to the primary instability region. Also, the MI may occur beyond the threshold power or the threshold frequency in the absence of the DRR, where the MI gains increase monotonously as the perturbation frequency Ω increases. It is worth noting that the DRR only influences the gain profiles in the additional regions $|\Omega| > \Omega_c$ and beyond the threshold power $P_{\rm th}$ and the threshold frequency $\tilde{\omega}_{\rm th}$, where the gain increases with the increasing τ_R; interestingly, the DRR has little scarcely effects on the MI gain in the primary regions for all four cases, where the self-steepening s_1 and the pseudo-quintic nonlinearity p_5 play a critical role in the gain, as shown in Figure 6. It can be also seen from Figure 6 that the peak gain $g_{\max}$ and the bandwidth remain unchanged for different DRR τ_R in primary instability regions, while the MI gain monotonously increase with τ_R in the additional instability regions. This means that the nonlinear competition of the self-steepening, the pseudo-quintic nonlinearity and the DRR results in an interesting feature that the self-steepening and the pseudo-quintic nonlinearity dominate the MI properties in the primary instability regions, while the DRR governs the MI properties in the additional instability regions. This may be explained by the fact that it is just the DRR that induces the MI in additional instability regions and naturally governs the distributions of the MI spectra. These novel features have never been disclosed in previous papers.

In addition, when the DRR is considered, MI can occur not only in the discussed-above four cases, but also in the other three regimes: in zero-GVD regimes of self-focusing and self-defocusing nonlinearity; in normal-GVD regime of self-focusing negative index region; and in abnormal-GVD regime of self-defocusing positive index region, respectively. For convenience, we call them Case E, F and G, respectively. It is easy to know that the MI gain in zero-GVD regimes of self-focusing and self-defocusing metamaterials are the same according to equation (8). The MI gain spectral profile with the initial power P_0 for Case E ($\tilde{\omega} = 0.707$) is presented in Figure 7a, which can be seen that the gain monotonous increases with both the initial power P_0 and the perturbation frequency Ω.

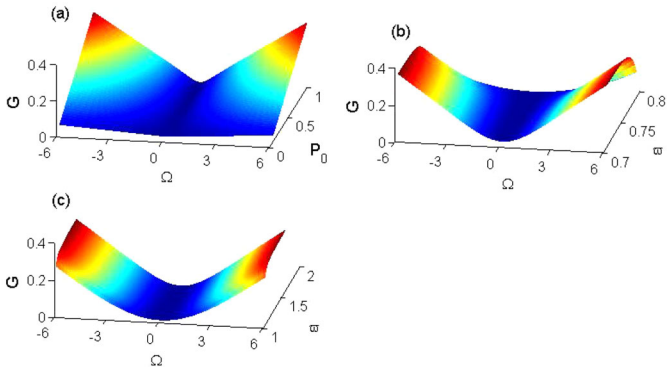

Fig. 7. Gain spectra profiles with $\tau_R = 0.03$ for (a) Case E $\tilde{\omega} = 0.707$; (b) Case F $P_0 = 1$ and (c) Case G $P_0 = 1$, respectively.

Figures 7b and 7c illustrate the gain spectral profiles with the corresponding $\tilde{\omega}$ for Case F and G, respectively. Quite different from the cases in absence of the DRR, the gain spectra for Case F and G are substantially altered by the DRR, exhibiting monotonous increase with the perturbation frequency Ω over the whole frequency band although the variations of gain with $\tilde{\omega}$ are different. On the whole, the spectral features of the MI induced by the DRR in these three cases are the same as those in conventional materials with the DRR [3], which suggest that the gain band may extend to unlimited high frequency. These results mean that it is also possible to observe MI at arbitrary high frequency and provide more ways of generating ultrashort pulses with ultrahigh repetition rate for future high-speed optical communication based on the metamaterials.

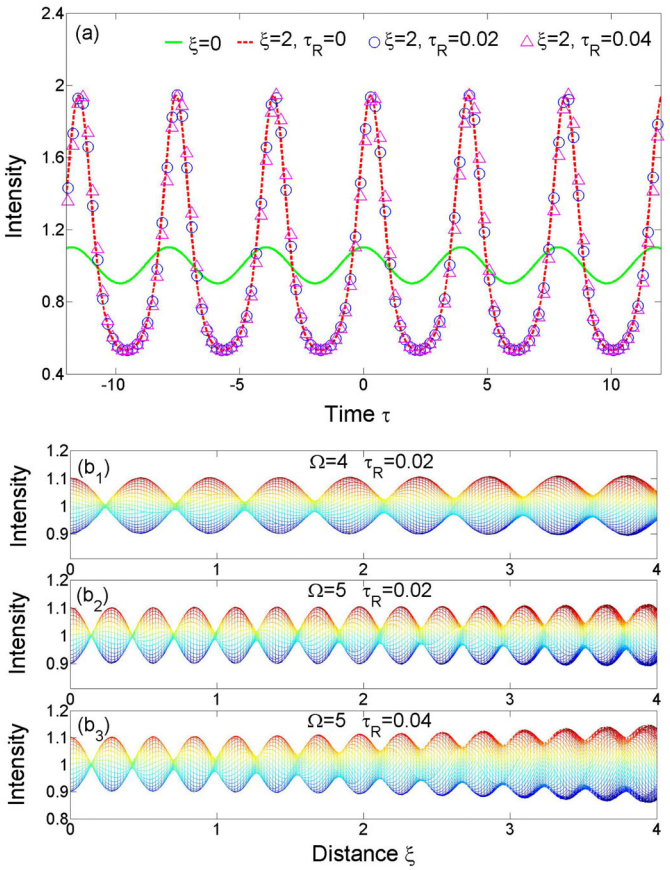

Fig. 8. Numerical evolutions of the modulated continuous wave in (a) the primary MI region at maximum modulation frequency $\Omega = 1.6$ and (b) the additional MI region of Case A, respectively.

4 Numerical confirmation

In this section, we numerically solve equation (2) to examine the MI induced by the self-steepening, the pseudo-quintic nonlinearity and the DRR by using the symmetric split-step Fourier method. The incident field is a cosinusoidally modulated continuous wave $U(0,\tau) = U_0[1 + a_0\cos(\Omega\tau)]$, where the perturbed wave is set to be $a_0 = 0.05$ and the initial amplitude of the background is set to be $U_0 = \sqrt{P_0}$ according to the different critical powers for different cases of MI.

Firstly, we simulate the evolution of the modulated continuous wave in primary and additional instability regions of Case A, as illustrated in Figure 8. To verify the analytical results, here we adopt the same self-steepening and pseudo-quintic nonlinearity parameters as in Figure 6a. In the primary MI region, for different DRR parameters τ_R, the modulated continuous wave has the same amplitudes after propagating a certain distance, as shown in Figure 8a. This confirms that the DRR scarcely influences the MI gain in primary MI region, which is in agreement with the results in Figure 6a. In the additional MI region, as shown in Figure 8b, the intensities of the modulated continuous wave appear a periodically oscillatory growth induced by the DRR with the propagation distance, and the higher the modulation frequency, the shorter the oscillating period; the lager the DRR parameter τ_R, the faster the amplitude increases, which also well coincide with the properties shown in Figure 6a.

Furthermore, we numerically confirm the modulation instabilities of the continuous wave for the other Case B, C and D in primary and additional MI regions, as shown in Figures 9a and 9b, respectively. Here we adopt the same initial powers P_0 and generalized frequencies $\tilde{\omega}$ as the corresponding cases in Figure 6 and take the modulation frequencies located in primary and additional regions for each case. From Figure 9a, it can be seen that in primary regions of each case, the distributions of the modulated waves in the presence of DDR are well coincident with those without DRR. As shown in Figure 9b, the numerical evolutions of the modulated continuous waves verify that the modulation instability can occur in the additional regions of Case B, C and D when the DRR is considered.

Finally, we simulate the evolutions of the modulated continuous waves for Case E, F and G, respectively, as shown in Figure 10. For Case E, the evolutions of the modulated continuous waves in zero-GVD regimes of both self-focusing and self-defocusing nonlinearity are almost the same by comparing Figure 10a with Figure 10b. For Case F in normal-GVD regime of self-focusing negative

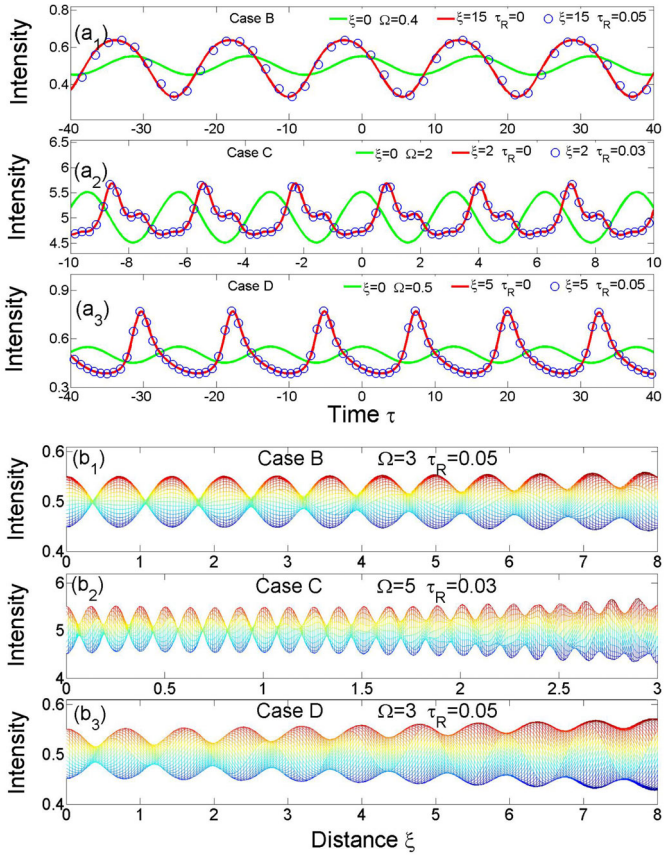

Fig. 9. Numerical evolution of the modulated continuous waves in (a) the primary and (b) the additional regions of Cases B, C and D. In addition to the parameters shown in the diagram, the other parameters are the same as in Figure 6.

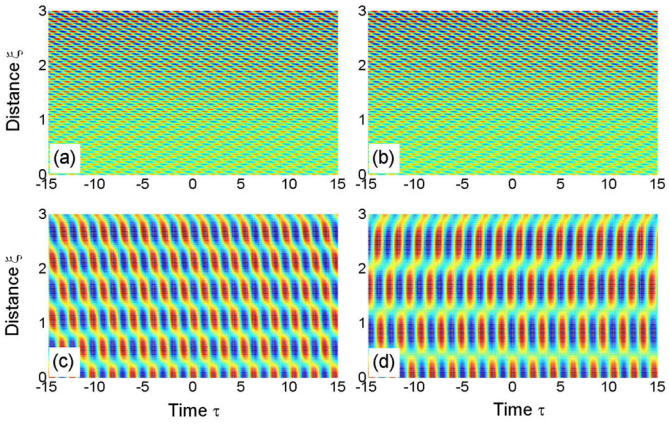

Fig. 10. Contours of the modulated continuous waves in (a) self-focusing ($\vartheta = 1$) and (b) self-defocusing ($\vartheta = -1$) nonlinearity of Case E $\tilde{\omega} = 0.707$ ($\beta_2 = 0$), in (c) Case F $\tilde{\omega} = 0.71$ ($\delta = 1, n < 0$) and (d) Case G $\tilde{\omega} = 1.2$ ($\delta = -1, n > 0$), respectively. The other parameters for all cases are adopted $P_0 = 1$, $\Omega = 3$ and $\tau_R = 0.04$.

index region and Case G in abnormal-GVD regime of self-defocusing positive index region, the continuous waves with the same Ω and τ_R show a similar evolution except for different velocities and period of oscillation that results from the different dispersion and nonlinear parameters.

5 Conclusions

To conclude, we have investigated the MI in metamaterials induced by the pseudo-quintic nonlinearity and the self-steepening effects along with the DRR in the framework of an extended NLS equation. By employing standard linear stability method, the analytical expression for MI gain is presented and the novel features of the MI are demonstrated in detail. Firstly, we considered the MI under the competition of the pseudo-quintic nonlinearity and the self-steepening effect in the absence of the DRR. It is found that MI can appear in four different cases: Case A in abnormal GVD regime of self-focusing negative index region; Case B in self-focusing positive index region; Case C in abnormal GVD regime of self-defocusing negative index region and Case D in normal GVD regime of self-defocusing negative index region. Compared to the MI gain spectra obtained for saturable nonlinearity, the MI gain shows more interesting dependence on the combinations of dispersion and nonlinearity and the competition of the pseudo-quintic nonlinearity and the self-steepening, exhibiting different threshold power and threshold frequency in each regions. This suggests that we can make the MI occur in different regions with different gains and the spectral widths by tuning the power and the frequency of the incident waves at will. It is very useful for generating solitary waves in different regions of dispersion and nonlinearity. Secondly, we discussed the influence of the DRR on the MI gain. It is found that when the DRR is considered, MI can occur not only in Cases A, B, C and D, but also in the other three cases: Case E in zero-GVD regimes of self-focusing or self-defocusing nonlinearity; Case F in normal-GVD regime of self-focusing negative index region; and Case G in abnormal-GVD regime of self-defocusing positive index region, respectively. For Cases A, B, C and D, the DRR leads to additional MI regions besides the primary ones, moreover, the DRR dominates the MI gain in the additional regions, while the self-steepening and the pseudo-quintic nonlinearity effects entirely govern the MI gain in primary ones. For Cases E, F and G, the MI gain exhibits monotonous growth with the perturbation frequency over the whole frequency band. These results mean that it is also possible to observe MI at arbitrary high frequency. Finally, we examined the analytical results by numerical simulations. The obtained results are useful in manipulating or tuning the MI gain in metamaterials and provide more ways to generate ultrashort pulses with ultrahigh repetition rate for high-speed optical communication.

Author contribution statement

Rongcao Yang carried out analytical derivation and theoretical analysis, Xuemin Min performed numerical simulations with Jinping Tian's help, Jinping Tian and Wenmei

Zhang involved the theoretical analysis and discussion. Rongcao Yang and Xuemin Min wrote the manuscript.

The authors would like to thank Prof. G.S. McDonald and Dr. J.M. Christian for useful discussions and helpful advice. This work is supported by the National Natural Science Foundation of China (NSFC) (Grants 61178013, 61271160), and Selected Project of Overseas Science and technology activities of Shanxi Province (Grant 201301).

References

1. A. Hasegawa, Opt. Lett. **9**, 288 (1984)
2. K. Tai, A. Hasegawa, A. Tomita, Phys. Rev. Lett. **56**, 135 (1986)
3. Y.S. Kivshar, G.P. Agrawal, *Optical Solitons: From Fibers to Photonic Crystals* (Academic Press, 2003)
4. G.P. Agrawal, P.L. Baldeck, R.R. Alfano, Phys. Rev. A **39**, 3406 (1989)
5. J.E. Rothenberg, Phys. Rev. A **42**, 682 (1990)
6. F.K. Abdullaev, S.A. Darmanyan, S. Bischoff, P.L. Christiansen, M.P. Sørensen, Opt. Commun. **108**, 60 (1994)
7. J.M. SotoCrespo, E.M. Wright, Appl. Phys. Lett. **59**, 2489 (1991)
8. W.P. Hong, Opt. Commun. **213**, 173 (2002)
9. G.L. Tiofack, A. Mohamadou, T.C. Kofané, A.B. Moubissi, Phys. Rev. E **80**, 066604 (2009)
10. N. Lazarides, G.P. Tsironis, Phys. Rev. E **71**, 036614 (2005)
11. M. Scalora, M.S. Syrchin, N. Akozbek, E.Y. Poliakov, G. D'Aguanno, N. Mattiucci, M.J. Bloemer, A.M. Zheltikov, Phys. Rev. Lett. **95**, 013902 (2005)
12. S. Wen, Y. Xiang, X. Dai, Z. Tang, W. Su, D. Fan, Phys. Rev. A **75**, 033815 (2007)
13. P.G. Li, R.C. Yang, Z.Y. Xu, Phys. Rev. E **82**, 046603 (2010)
14. Y. Xiang, X. Dai, S. Wen, J. Guo, D. Fan, Phys. Rev. A **84**, 033815 (2011)
15. G. D'Aguanno, N. Mattiucci, M. Scalora, M.J. Bloemer, Phys. Rev. Lett. **93**, 213902 (2004)
16. M. Marklund, P.K. Shukla, L. Stenflo, Phys. Rev. E **73**, 037601 (2006)
17. R.C. Yang, Y. Zhang, J. Opt. Soc. Am. B **28**, 123 (2011)
18. S. Loomba, M.S.M. Rajan, R. Gupta, A. Mahalingam, Eur. Phys. J. D **68**,130 (2014)
19. S. Wen, Y. Xiang, W. Su, Y. Hu, X. Fu, D. Fan, Opt. Express **14**, 1568 (2006)
20. Y. Xiang, S. Wen, X. Dai, Z. Tang, W. Su, D. Fan, J. Opt. Soc. Am. B **24**, 3058 (2007)
21. Y. Xiang, X. Dai, S. Wen, D. Fan, J. Opt. Soc. Am. B **28**, 908 (2011)
22. G.L. Tiofacka, A. Mohamadou, Alim, K. Porsezian, T.C. Kofane, J. Mod. Opt. **59**, 972 (2012)
23. M. Saha, A.K. Sarma, Opt. Commun. **291**, 321 (2013)
24. X. Zhong, K. Cheng, K. Chiang, J. Opt. Soc. Am. B **31**, 1484 (2014)
25. D. Boardman, O. Hess, R.C. Mitchell-Thomas, Y.G. Rapoport, L. Velasco, Photon. Nanostruct. **8**, 228 (2010)
26. M.J. Potasek, Opt. Lett. **12**, 921 (1987)
27. S. Wen, W. Su. H. Zhang, X. Fu, L. Qian, D. Fan, Chin. Phys. Lett. **20**, 853 (2003)
28. P. Tchofo Dinda, C.M. Ngabireng, K. Porsezian, B. Kalithasan, Opt. Commun. **266**, 142 (2006)
29. J.B. Pendry, A.J. Holden, D.J. Robbins, W.J. Stewart, IEEE Trans. Microwave Theory Technol. **47**, 2075 (1999)
30. R. Smith, W.J. Padilla, D.C. Vier, S.C. Nemat-Nasser, S. Schultz, Phys. Rev. Lett. **84**, 4184 (2000)
31. A.K. Popov, V.M. Shalaev, Opt. Lett. **31**, 2169 (2006)
32. L. Sun, X. Yang, J. Gao, Appl. Phys. Lett. **103**, 201109 (2013)
33. T. Lepetit, É. Akmansoy, J.-P. Ganne, Appl. Phys. Lett. **95**, 121101 (2009)
34. V.M. Shalaev, W. Cai, U.K. Chettiar, H.-K. Yuan, A.K. Sarychev, V.P. Drachev, A.V. Kildishev, Opt. Lett. **30**, 3356 (2005)